ResearchGate

See discussions, stats, and author profiles for this publication at: https://www.researchgate.net/publication/228523795

Monolayer-Protected Cluster Superlattices: Structural, Spectroscopic, Calorimetric, and Conductivity Studies

ARTICLE *in* CHEMISTRY OF MATERIALS · DECEMBER 2000

Impact Factor: 8.35 · DOI: 10.1021/cm990429t

CITATIONS
66

READS
29

13 AUTHORS, INCLUDING:

SANDHYARANI N
National Institute of Technology Calicut
45 PUBLICATIONS **758** CITATIONS
SEE PROFILE

M. P. Antony
Indira Gandhi Centre for Atomic Research
86 PUBLICATIONS **643** CITATIONS
SEE PROFILE

Pandian Kannaiyan
University of Madras
88 PUBLICATIONS **618** CITATIONS
SEE PROFILE

Pradeep Thalappil
Indian Institute of Technology Madras
347 PUBLICATIONS **8,810** CITATIONS
SEE PROFILE

Available from: Pandian Kannaiyan
Retrieved on: 16 January 2016

Monolayer-Protected Cluster Superlattices: Structural, Spectroscopic, Calorimetric, and Conductivity Studies

N. Sandhyarani,[†,‡] M. R. Resmi,[†,‡] R. Unnikrishnan,[†,‡] K. Vidyasagar,[‡] Shuguang Ma,[§] M. P. Antony,[∥] G. Panneer Selvam,[∥] V. Visalakshi,[⊥] N. Chandrakumar,[⊥] Kannaiyan Pandian,[#] Yu-Tai Tao,[#] and T. Pradeep*[,†,‡]

Department of Chemistry and Regional Sophisticated Instrumentation Centre, Indian Institute of Technology, Madras 600 036, India; Department of Chemistry, Purdue University, West Lafayette, Indiana 47907; Radiochemistry Laboratory, Indira Gandhi Centre for Atomic Research, Kalpakkam, India; Central Leather Research Institute, Madras 600 020, India; and Institute of Chemistry, Academia Sinica, Taipei, Taiwan, Republic of China

Received July 12, 1999. Revised Manuscript Received October 19, 1999

Alkanethiol-protected silver clusters of average diameter 4.0 ± 0.5 nm form single-phase superlattice solids, and their X-ray powder diffractograms have been fully indexed to single cubic unit cells. Whereas alkanethiols with five or more carbon atoms form superlattices, the corresponding cluster with four carbons yield only separated clusters. The superlattice solids can be recrystallized from nonpolar solvents. No such superlattices are seen for the corresponding gold clusters. The superlattice collapses upon heating, but the solid retains the structure even at 398 K, much above the melting point of crystalline alkanes and the corresponding self-assembled monolayer. In situ variable-temperature X-ray diffraction investigations did not show any solid-state phase transitions in the superlattice. Temperature-dependent infrared spectroscopy reveals the melting of the alkyl chain, and it is seen that the chain as a whole achieves rotational freedom prior to the collapse of the superlattice. Calorimetric investigations show distinct monolayer and superlattice melting transitions. The chemical nature of the cluster−molecule interaction is similar to that of the previously investigated gold and silver systems, as revealed by NMR, mass, infrared, and X-ray photoelectron spectroscopies and thermogravimetry analyses. Conductivity measurements clearly manifest the superlattice melting transition. Diffusion constants in solution measured by NMR show that the relative decrease in the diffusion constant with increasing monolayer chain length is smaller for silver than for gold, suggested to be a signature of intercluster interaction even in solution. Corroborative evidence is provided by the variable-temperature UV/vis investigations of the clusters.

Introduction

Monolayer-protected clusters (MPCs)[1] are important nanophase materials due to their diverse chemical and physical properties and potential applications.[2] Because the specificity of the chemistry can be used to attach molecules of choice at different surfaces, a large variety of metal clusters have been synthesized.[3] Different cluster dimensions can be prepared by appropriate manipulation of synthetic parameters.[4] Although the properties of the core are immensely important,[5] the chemistry of the monolayers themselves has also attracted attention in the recent past.[1] The diversity of the chemistry of self-assembled monolayers[6] (SAMs) grown on planar surfaces (2D SAMs) can be directly adapted to monolayers on cluster surfaces (3D SAMs).[7,8]

* E-mail: pradeep@iitm.ernet.in. Fax: ++91 44 235 0509 or 2545.
† Regional Sophisticated Instrumentation Centre.
‡ Department of Chemistry, Indian Institute of Technology.
§ Purdue University.
∥ Indira Gandhi Centre for Atomic Research.
⊥ Central Leather Research Institute.
Academia Sinica.

(1) For a recent review of the area, see: Hostetler, M. J.; Murray, R. W. *Curr. Opin. Colloid Interface Sci.* **1997**, *2*, 42−50.
(2) (a) Wang, Y.; Herron, N. *J. Phys. Chem.* **1991**, *95*, 525−532. (b) Schmid, G. *Chem. Rev.* **1992**, *92*, 1709−1727. (c) Schon, G.; Simon, U. *Colloid Polym. Sci.* **1995**, *273*, 101−117. (d) Schon, G.; Simon, U. *Colloid Polym. Sci.* **1995**, *273*, 202−218.
(3) (a) Brust, M.; Walker, M.; Bethell, D.; Schiffrin, D. J.; Whyman, R. *J. Chem. Soc., Chem. Commun.* **1994**, 801−802. (b) Vijaya Sarathy, K.; Raina, G.; Yadav, R. T.; Kulkarni, G. U.; Rao, C. N. R. *J. Phys. Chem. B* **1997**, *101*, 9876−9880 (c) Reetz, M. T.; Helbig, W. *J. Am. Chem. Soc.* **1994**, *116*, 7401−7402. (d) Duteil, A.; Schmid, G.; Meyer-Zeika, W. *J. Chem. Soc., Chem. Commun.* **1995**, 31−32.
(4) Hostetler, M. J.; Wingate, J. E.; Zhong, C.-J.; Harris, J. E.; Vachet, R. W.; Clark, M. R.; Londono, J. D.; Green, S. J.; Stokes, J. J.; Wignall, G. D.; Glish, G. L.; Porter, M. D.; Evan, N. D.; Murray, R. W. *Langmuir* **1998**, *14*, 17−30.
(5) (a) Alivisatos, A. P. *Science* **1996**, *271*, 933−937. (b) Shi, J.; Gider, S.; Babcock, K.; Awschalom, D. D. *Science* **1996**, *271*, 937−941.
(6) Ulman, A. *An Introduction to Ultrathin Organic Films: From Langmuir Blodgett to Self-Assembly*; Academic Press: New York, 1991; *Chem. Rev.* **1996**, *96*, 1533−1554.
(7) Terril, R. H. et al. *J. Am. Chem. Soc.* **1995**, *117*, 12537−12548. (b) Leff, D. V.; Ohara, P. C.; Heath, J. R.; Gelbart, W. M. *J. Phys. Chem.* **1995**, *99*, 7036−7041. (c) Leff, D. V.; Brandt, L.; Heath, J. R. *Langmuir* **1996**, *12*, 4723−4730. (d) Hostetler, M. J.; Stokes, J. J.; Murray, R. W. *Langmuir* **1996**, *12*, 3604−3612. (e) Johnson, S. R.; Evans, S. D.; Mahon, S. W.; Ulman, A. *Langmuir* **1997**, *13*, 51−57. (f) Alvarez, M. M.; Khoury, J. T.; Schaaff, T. G.; Shafigullin, M. N.; Vezmar, I.; Whetten, R. L. *J. Phys. Chem. B* **1997**, *101*, 3706−3712.
(8) (a) Hostetler, M. J.; Green, S. J.; Stokes, J. J.; Murray, R. W. *J. Am. Chem. Soc.* **1996**, *118*, 4212−4213. (b) Badia, A.; Cuccia, L.; Demers, L.; Morin, F.; Lennox, R. B. *J. Am. Chem. Soc.* **1997**, *119*, 2682−2692.

10.1021/cm990429t CCC: $19.00 © 2000 American Chemical Society
Published on Web 12/23/1999

The advantage of high monolayer concentration owing to large surface area has made it possible to investigate them by a host of analytical techniques, which is difficult with 2D monolayers. Thus, there have been structural and spectroscopic studies.[7,8] Electrical transport properties,[9] phase transitions of the alkyl chains,[10] reactivity of the terminal groups,[11] and exchange behavior of the adsorbates[12] have all been studied. Most of these investigations have centered on Au−alkanethiol system, chiefly because of the wealth of knowledge of the corresponding 2D SAMs.[13,14] However, relatively little knowledge exists on the corresponding Ag system, although there are studies on some of the important aspects such as structure, cluster size, self-organization, and so on.[15−17]

The objectives of this work have been to (1) make super structures of the clusters in the solid state through interaction of the monolayers, (2) investigate such structures by a host of analytical techniques, and (3) compare the superstructures with the corresponding separated cluster systems.

Experimental Section

Materials. $AgNO_3$ (Merck, 99.99%), $HAuCl_4 \cdot 3H_2O$ (CDH, 99.8%), tetra-*n*-octylammonium bromide (Merck, 98%), $NaBH_4$, octadecanethiol, octanethiol, pentanethiol, and butanethiol (all Aldrich, 99%) were used as received. AR grade solvents and deionized and subsequently distilled water were used.

Synthetic Procedure. Octadecane-, octane-, pentane-, and butanethiol-protected clusters were synthesized using a modified literature method described originally for gold clusters;[7e] these will be referred to later as C18 (Ag−ODT), C8 (Ag−OT), C5 (Ag−PT), and C4 (Ag−BT) clusters, respectively. Briefly, 0.0358 M toluene solution (21.6 mL) of tetra-*n*-octylammonium bromide was added to a vigorously stirred 0.0288 M aqueous solution (10 mL) of $AgNO_3$. After 1 h of stirring, a 0.0139 M toluene solution (23.8 mL) of the respective thiol was added, and the resulting solution was stirred for 10 min. To this, a 8.25 mL aqueous solution (0.2378 M) of sodium borohydride was added dropwise. Reduction and derivatization of silver is evidenced by the brown color of the toluene phase, which was originally colorless. The solution was stirred overnight, and the organic layer was separated. It was allowed to evaporate slowly to 10 mL (this took several hours to a few days at the ambient temperature), and 100 mL of methanol was added in order to precipitate the cluster. The material was washed several times with methanol and was air-dried. It was stored in ambient laboratory air, and no significant change in the spectroscopic properties was observed in the time scale of 2 months. However, heated samples seem to degrade with time. The material was found to be composed of a mixture of isolated clusters (freely soluble in organic solvents, almost instantaneously) and superlattice crystallites (partly soluble in organic solvents, complete dissolution took longer times). Both of these were subjected to transmission electron microscopy (TEM), optical absorption, and XRD. However, in the results presented below, unless otherwise stated, we have used the material as prepared without separation because both were composed of the same constituents. A similar procedure was employed for Au clusters as well.

Ag−octanethiolate-layered materials[18] were synthesized using a two-phase method.[18a] Briefly, a toluene solution of octanethiol was added to a vigorously stirred aqueous solution of $AgNO_3$ (Ag:thiol ratio of unity) and stirred for 3 h. Ag−octanethiolate formed as a white suspension in toluene. The solid was collected and washed with toluene and water to remove unreacted thiol and $AgNO_3$, respectively. The aqueous solution was free of Ag^+ ions. A comparative study of thiolates and the cluster superlattices, focusing on their melting behavior, will be published separately.[19]

X-ray Diffraction. Several X-ray diffractometers (Cu Kα) were used. The samples were spread on antireflective glass slides. The films were wetted with acetone for uniformity and were blown dry before measurement. The use of acetone did not affect the measurements, which was confirmed with a pressed pellet. For variable-temperature measurements, a Philips X′ Pert-MPD diffractometer was used. At each temperature, the sample was allowed to stabilize for 3 min and the diffractogram in the range of 3−51° (2θ) was measured. A step size of 0.05° was used.

Transmission Electron Microscopy. The initial micrographs were taken with a 200 kV JEOL JEM-2000EX microscope at Purdue University. The Ag cluster images presented here were taken with a Philips 120 kV machine. Drop-cast films of the clusters were prepared on carbon-coated Cu grids. To observe ordered structure of the clusters, slow evaporation of the solvent was necessary (the specimens were prepared in a cold room maintained at 277 K). Superlattice crystallites were dispersed in toluene by sonication, and TEM specimens were prepared by drop-casting.

Atomic Force Microscopy (AFM). An Autoprobe AFM (Park Scientific Instruments) equipped with a 10 μm scan head was used. Images were taken in the contact mode. All images were acquired in air with a Si_3N_4 cantilever of 0.6 μm radius.

Scanning Electron Microscopy. A JSM-5400 JEOL scanning electron microscope at an accelerating voltage of 30.0 kV was used. The surface was coated with a thin film of Pt before imaging.

X-ray Photoelectron Spectroscopy. X-ray photoelectron spectroscopic measurements were carried out with a VG ESCALAB MkII spectrometer with Mg Kα radiation. No charging was observed.

Infrared Spectroscopy. Infrared spectra (dispersed in KBr) were measured with a Bruker IFS 66v FT-IR spectrometer. All spectra (2 cm^{-1} resolution) were averaged over 200 scans. Variable-temperature measurements were performed with a home-built heater and a programmable temperature controller.

Mass Spectrometry. Positive-ion mass spectra (electron impact, 70 eV) were measured with a Finnigan TSQ 700 triple quadrupole mass spectrometer at Purdue University. The

(9) Ingram, R. S.; Hostetler, M. J.; Murray, R. W.; Schaaff, T. G.; Khoury, J. T.; Whetten, R. L.; Bigioni, T. P.; Guthrie, D. K.; First, P. N. *J. Am. Chem. Soc.* **1997**, *119*, 9279−9280.

(10) Badia, A.; Singh, S.; Demers, L.; Cuccia, L.; Brown, G. R.; Lennox, R. B. *Chem. Eur. J.* **1996**, *2*, 359−363.

(11) Templeton, A. C.; Hostetler, M. J.; Kraft, C. T.; Murray, R. W. *J. Am. Chem. Soc.* **1998**, *120*, 1906−1911.

(12) Ingram, R. S.; Hostetler, M. J.; Murray, R. W. *J. Am. Chem. Soc.* **1997**, *119*, 9175−9178. (b) Hostetler, M. J.; Templeton, A. C.; Murray, R. W. *Langmuir* **1999**, *15*, 3782−3789.

(13) (a) Bain, C. D.; Troughton, E. B.; Tao, Y. T.; Evall, J.; Whitesides, G. M.; Nuzzo, R. G. *J. Am. Chem. Soc.* **1989**, *111*, 321−335. (b) Finkelea, H. O.; Avery, S.; Lynch, M. *Langmuir* **1987**, *3*, 409−413. (c) Allara, D. L.; Nuzzo, R. G. *Langmuir* **1985**, *1*, 52−56.

(14) (a) Porter, M. D.; Bright, T. B.; Allara, D. L.; Chidsey, C. E. D. *J. Am. Chem. Soc.* **1987**, *109*, 3559−3568. (b) Nuzzo, R. G.; Fusco, F. A.; Allara, D. L. *J. Am. Chem. Soc.* **1987**, *109*, 2358−2568.

(15) (a) Korgel, B. A.; Fitzmaurice, D. *Adv. Mater.* **1998**, *10*, 661−664. (b) Wang, Z. L.; Harfenist, S. A.; Vezmar, I.; Whetten, R. L.; Bently, J.; Evans, N. D.; Alexander, K. B. *Adv. Mater.* **1998**, *10*, 808−812. (c) Harfenist, S. A.; Wang, Z. L.; Whetten, R. L.; Vezmar, I.; Alvarez, M. A. *Adv. Mater* **1997**, *14*, 817−822. (d) Ohara, P. C.; Heath, J. R.; Gelbert, W. M. *Angew. Chem., Int. Ed. Engl.* **1997**, *36*, 1078−1080. (e) Harfenist, S. A.; Wang, Z. L.; Alvarez, M. M.; Vezmar, I.; Whetten, R. L. *J. Phys. Chem.* **1996**, *100*, 13904−13910.

(16) Kang, S. Y.; Kim, K. *Langmuir* **1998**, *14*, 226−230.

(17) Patil, V.; Mayya, K. S.; Pradhan, S. D.; Sastry, M. *J. Am. Chem. Soc.* **1997**, *119*, 9281−9282.

(18) (a) Bensebaa, F.; Ellis, T. H.; Kruus, E.; Voicu, R.; Zhou, Y. *Langmuir* **1998**, *14*, 6579−6587. (b) Parikh, A. N.; Gillmor, S. D.; Beers, J. D.; Beardmore, K. M.; Cutts, R. W.; Swanson, B. I. *J. Phys. Chem.* **1999**, *103*, 2850−2861. (c) Dance, I. G.; Fisher, K. J.; Herath Bamda, R. M.; Scudder, M. L. *Inorg. Chem.* **1991**, *30*, 183−187.

(19) Sandhyarani, N.; Antony, M. P.; Paneer Selvam, G.; Pradeep, T. *Langmuir*, submitted for publication.

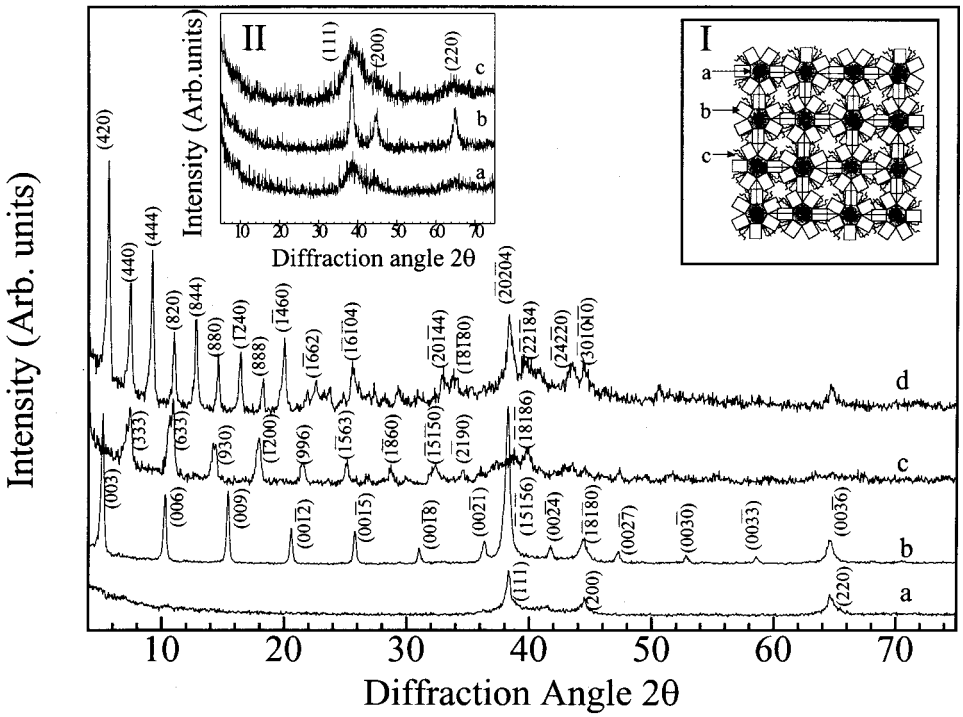

Figure 1. Cu Kα XRD patterns of (a) Ag−BT, (b) Ag−PT, (c) Ag−OT, and (d) Ag−ODT. A schematic of the superlattice is shown in inset I. The cluster cores and the organized and unorganized alkyl chains are represented by a, b, and c, respectively. The shape of the cluster cores observed in TEM[15] and the ordering of the alkyl chains seen in IR are considered in preparing this schematic. Inset II shows the XRD patterns of the Au clusters capped with (a) BT, (b) OT, and (c) ODT. The reflections are labeled.

samples were introduced with a solid probe and were heated from 298 to 1200 K as per a programmed-temperature ramp.

Differential Scanning Calorimetry and Thermogravimetry. DSC data were taken with a Netzsch PHOENIX DSC204 instrument. Samples (10 mg) encapsulated in aluminum pans were used. The measurements were conducted in the temperature range of 123−473 K. TG data were acquired with a Netzsch STA 409. About 10 mg of the samples were used. Data in the range of 298−873 K (scan speed of 10 K/min) were measured. The samples left behind after TG analysis were metal powders.

Conductivity. Two- and four-probe resistance measurements were conducted with a Keithley-2001 nanovoltmeter/current source. Temperature-dependent data were acquired with a home-built heater. Contacts were made with silver paint on molten and compacted (3000 lbs) pellets (13 mm diam.).

Optical Absorption Spectroscopy. Optical absorption spectra were collected with a Varian Cary 5 UV/vis/NIR spectrophotometer. Low-temperature measurements were conducted in a nitrogen atmosphere. The transmission spectra of solids were measured by depositing drop-cast films on quartz windows.

Nuclear Magnetic Resonance Spectroscopy. Proton NMR spectra were recorded with a JEOL GSX 400 NMR instrument. Solutions were prepared in $CDCl_3$, and measurements were conducted at room temperature. Variable-temperature measurements were performed with a mixture of CCl_4 and $CDCl_3$. Diffusion coefficient measurements were conducted with a Bruker MSL 300 P instrument. Clusters (50 mg) were dissolved in 0.5 mL of $CDCl_3$. The methodology has been reported in the literature.[20]

Results and Discussion

This section is divided into two parts: solid and solution states.

Investigations in the Solid State. *X-ray Diffraction*. Figure 1 shows the X-ray diffractograms of C4-, C5-, C8-, C18-protected silver clusters. Whereas the C4 cluster shows only the (111), (200), and (220) reflections of the silver metal, the diffractograms of C5, C8, and C18 clusters show additional reflections. All of them show characteristic low-angle peaks corresponding to larger unit cells. Such a lattice composed of alkanethiolate-capped silver clusters can only result from the periodic arrangement of these clusters.[21] Therefore, we proceeded to indexing the pattern with unit cell dimensions larger than the core cluster size revealed by TEM (see below). All of the reflections can be indexed to simple cubic unit cells, which are labeled in the figure. In C5, most of the reflections are (00*l*) type giving one of the lattice parameters as 52.023 Å. Including the parent silver reflections also in the pattern, a simple cubic cell of the same dimension can be inferred. In Ag−OT and Ag−ODT, mixed (*hkl*) reflections are observed that can be assigned to cubic unit cells with $a = 59.172$ and 67.465 Å, respectively. Important aspect of the patterns is that even the bulk Ag reflections also become part of the superlattice reflections. In the case of Ag−PT, this is particularly clear. It may be noted that all of the reflections can be fitted to the predicted structures, indicating that the powder material is largely single phase. For Ag−OT and Ag−ODT, reflections of the isolated clusters are not completely absent. For comparison, the XRD patterns of the corresponding Au clusters are shown in inset II of Figure 1, which show only the bulk Au reflections. The particle diameter of Au−ODT obtained from Scherrer formula[22] (29 Å) was

(20) (a) Sendhil Velan, S.; Chandrakumar, N. *Proc. Indian Acad. Sci. (Chem. Sci.)* **1994**, *106*, 1661−1669. (b) Sendhil Velan, S.; Chandrakumar, N. *J. Magn. Reson.* **1996**, *123*, 122−125.

(21) Whetten, R. L.; Shaffigullin, M. N.; Khoury, J. T.; Schaaf, T. G.; Vezmar, I.; Alvarez, M. M.; Wilkinson, A. *Acc. Chem. Res.* **1981**, *14*, 397−406.

in close agreement with that from TEM (30 ± 5 Å, see below). Although the diameter of the Ag clusters from TEM is not greatly different, the diffraction peaks are narrower, suggesting that the particles are composed of several superlattice unit cells.

It may be noted that the diffraction pattern is also compatible with cubic unit cells whose *a* parameter is one-third (C5 and C8) or half (C18) of the reported value. However, such a unit cell parameter will not be compatible with the TEM data, which shows that the cluster core diameter itself is 40 ± 5 Å. It is also known from other spectroscopic data that there are no adventitious contaminants present in the sample explaining the features in the XRD patterns. In addition, in the studies to be discussed below, it will be shown that the material is composed of individual alkanethiol-capped clusters. The superlattice solid can be prepared from solutions where the clusters are present in the separated form. Alternate ways of indexing the pattern were not successful.

We attribute the superlattice formation to the interdigitation of the alkyl chains. Widths of the reflections are smaller than the Au counterpart. Taking the effective core cluster dimension from TEM (see below) and all-trans arrangement of the alkyl chain (as seen in infrared spectroscopy, see below), a model for the superlattice can be easily arrived at. By assuming the cluster core size to be similar for all the clusters (i.e., 40 Å), the sum of core cluster diameter and twice the alkyl chain length works out to 58.1, 65.4, and 90.4 Å, respectively for Ag−PT, Ag−OT, and Ag−ODT. The calculation assumed C−C, C−S and Ag−S bond lengths to be 1.54, 1.81, and 2.56 Å, respectively. Thus, the unit cell dimensions are less than the sum of the cluster core diameter and twice the length of the alkyl chains**.** This suggests that approximately 4, 5, and 18 CH_2's, respectively, are interdigitating in these clusters. Although uncertainties in measuring cluster core size and the extent of tilt of the alkyl chains contribute to errors in calculating the actual number of interdigitated methylenes, it is clear that this number is not a constant and is not linear with chain length. This can happen only if bundles of alkyl chains interdigitate. Interdigitation of individual alkyl chains alone could lead to a high degree of disorder, which is not manifested in IR investigations (see below). Schematic of such a solid is shown in inset I of Figure 1.

Layered Ag−octanethiolates have been the subject of earlier studies,[18] and it has been shown that there is no interdigitation of the alkyl chains. The XRD patterns of the cluster superlattice and the Ag−thiolates are similar, but the *d* spacing is less in the former, again due to interdigitation.[19]

In Situ Variable-Temperature XRD. To see the structural transitions of the superlattice solid, we investigated the variable-temperature X-ray powder diffraction pattern of the clusters. In the following, we present the data of Ag−OT, although we have performed similar measurements on all of the other systems. The powder diffraction pattern as a function of temperature is shown in Figure 2. The patterns also show a few additional reflections due to the sample holder, which are marked

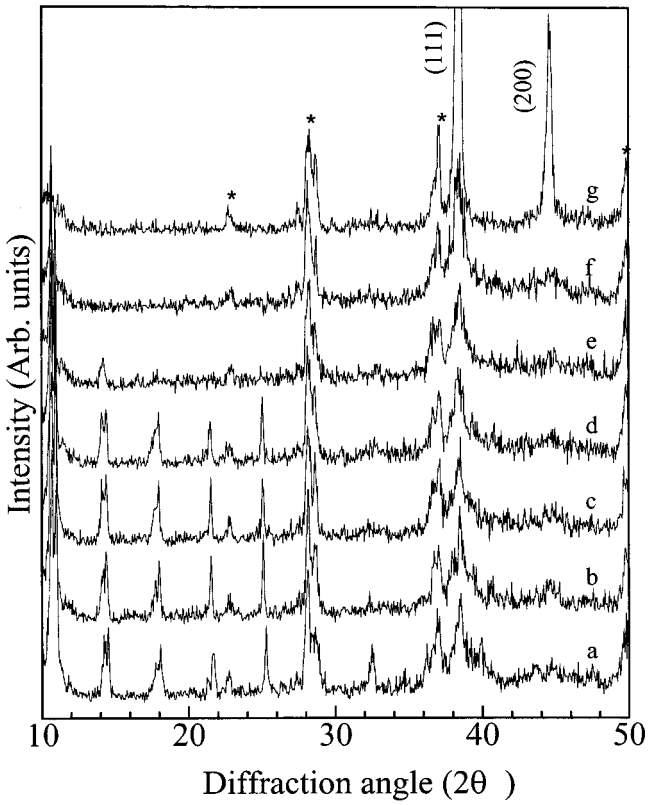

Figure 2. Variable-temperature Cu Kα powder diffraction patterns of Ag−OT at (a) 298 K (b) 348, (c) 373, (d) 398, (e) 423, (f) 448, and (g) 473. The peaks labeled * (asterisk) are due to the sample holder.

with asterisks (*). To compare the spectra, all of the diffractograms were acquired under the same experimental conditions, and the intensities of the spectra were not manipulated for presentation, except for being offset for clarity. It can be seen that the superlattice reflections begin to disappear at 398 K, and the peaks are almost lost at 423 K at which temperature individual Ag cluster reflections begin to attain prominence. At 448 K, the superlattice peaks are completely lost, and at 473 K, only the bulk metal peaks appear in the pattern. Note that these peaks have increased in intensity significantly at this temperature. This is attributed to the annealing of the cluster cores. Upon cooling of the sample back to room temperature, no superlattice peaks reappeared (not shown), but the bulk metal peaks retained their intensities. However, when the sample was heated to 423 K and subsequently cooled to room temperature, all of the superlattice peaks reappeared.

What comes out of this measurement is that the superlattice is a crystalline solid even above the alkyl chain melting transition, which is observed below 373 K in normal alkanes[23] and in 2D SAMs.[24] This means that intercluster interaction (mostly through the alkyl chains) is significant. Even after the collapse of the superlattice, it can regain order upon cooling, indicating that alkyl chain mobility within the molten state is

(22) West, A. R. *Solid State Chemistry and its Applications*; John Wiley and Sons: New York, 1987.

(23) For phase transitions in alkanes, see: Maroncelli, M.; Qi, S. P.; Strauss, H. L.; Snyder, R. G. *J. Am. Chem. Soc.* **1982**, *104*, 6237−6247.

(24) For example, see: Sandhyarani, N.; Pradeep, T. *Vacuum* **1998**, *49*, 279−284.

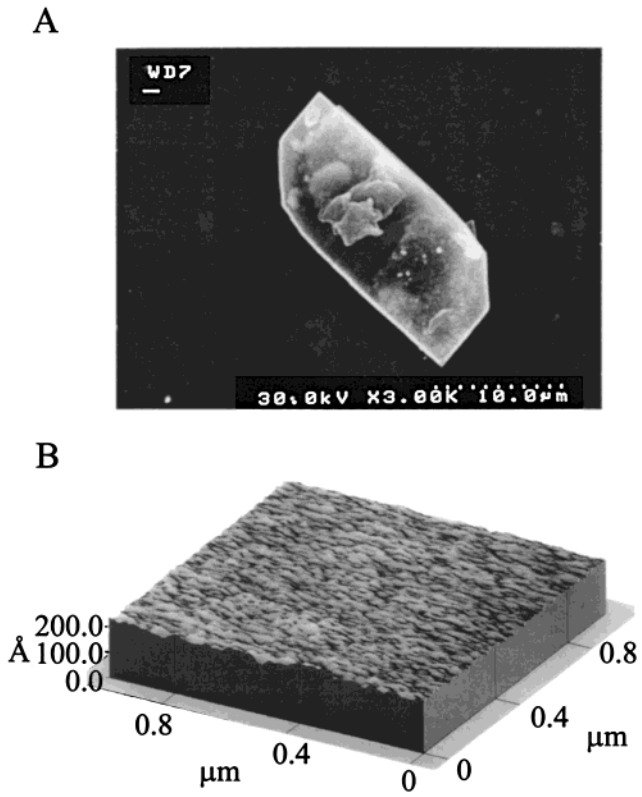

Figure 3. (A) Scanning electron micrograph of a crystallite of Ag−OT. (B) AFM image of the surface of a superlattice crystallite. Note that the surface roughness is within tens of angstroms.

restricted and orientational freedom is limited. The superlattice solid does not exhibit any other solid phase other than the simple cubic phase.

Scanning Electron Microscopy. The scanning electron micrograph of a crystallite of the superlattice in a dropcast film is shown in Figure 3A. The preparation was done on a freshly cleaved mica film. The crystallite is about 20 μm in length and 5 μm in width and depth. Although several morphologies are found in SEM, rodlike shapes are typical. The same crystallites were imaged by optical microscopy as well. The crystallites looked brown-black to the naked eye.

Atomic Force Microscopy. A topographic image of the surface of a crystallite (prepared by drop casting on freshly cleaved mica) is shown in Figure 3B. The resolution is inadequate to observe isolated clusters. However, the surface of the crystallite is smooth, and the surface roughness is within tens of angstroms, as expected.

Transmission Electron Microscopy. TEM gives a statistical description of the size and shape of the particles. In Figure 4, we show the transmission electron micrographs of (A) a dropcast film of Ag−OT and (B) a superlattice crystallite (deposited from a suspension). An analysis shows that the size distribution is more uniform in B, with an average size of 4 ± 0.5 nm. However, the superlattice order is not observed in this image although there are regions extending over a few clusters where periodicity is observed. In A, a wider distribution of cluster sizes is seen, as expected because it is prepared from solution. However, there are regions (marked in the figure) where translational periodicity is observed. In all of these regions, hexagonal packing

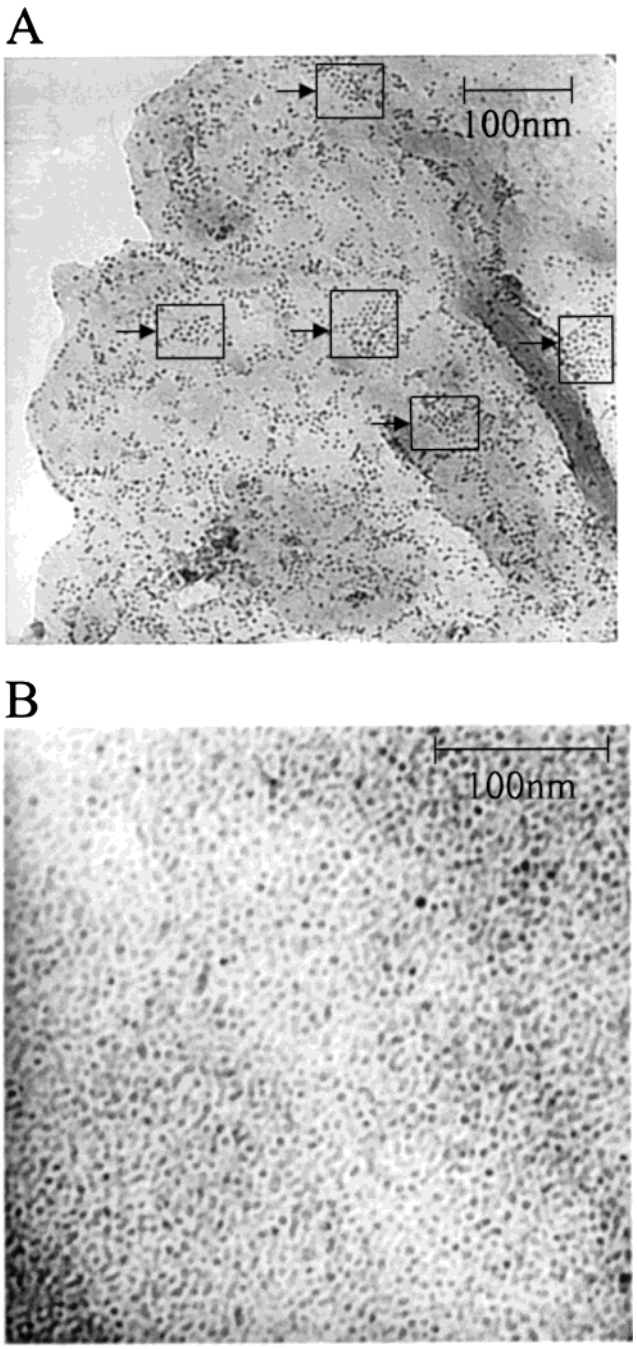

Figure 4. Transmission electron micrographs of octanethiol-capped Ag cluster. (A) Soluble portion of Ag−OT and slow evaporation leading to ordering. The observed (111) planes are marked. Absence of a long-range order is attributed to the polydispersity of the particles. (B) Insoluble portion after sonication in toluene. Uniform size distribution is observed.

is observed corresponding to (111) planes. This shows that crystallization from the solution phase is possible. TEM investigations of these superlattices are well-documented in the literature.[15] Our TEM observations can be summarized as follows. (1) Superlattice structures are not seen in the crystallites of Ag−OT, possibly due to the melting of the monolayer-assembled cluster solid in the electron beam (see below). It appears that in larger crystallites melting occurs rather quickly. We have seen that the melting of the crystallites is almost instantaneous upon exposure to the electron beam as expected in a hydrocarbon-assembled solid. However,

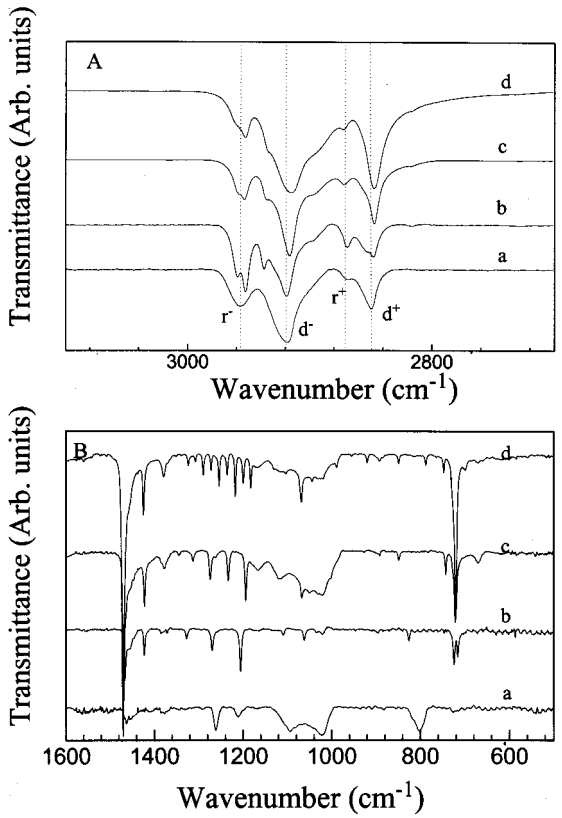

Figure 5. (A) High- and (B) low-frequency FT-IR spectra of (a) Ag−BT, (b) Ag−PT, (c) Ag−OT, and (d) Ag−ODT.

it is possible to see order extending over to tens of clusters in monolayer films of the clusters. The particles as prepared are not monodisperse, but in the crystallites, they are remarkably uniform in size, as required. (2) In Ag−BT (not shown), the particle size is larger (shown by XRD peak widths). Particles of assorted shapes are seen in Ag−BT, whereas Ag−OT and Ag−ODT are more uniform. This may be one of the reasons why a superlattice is not observed in Ag−BT. (3) Many of the clusters in both Ag−OT and Ag−BT show Moirè fringes, indicating that the electron beam undergoes interference from different crystallographic planes. In Au clusters, atomic lattices have been imaged (not shown), indicating that the individual clusters are tiny single crystals.

X-ray Photoelectron Spectroscopy. $Ag3d_{5/2}$ and $Ag3d_{3/2}$ appear at around 368 and 374 eV, respectively. For all of the clusters, the peaks lie within ±0.5 eV. This value corresponds to Ag(0). There was no asymmetry in the peak shape, indicating that all the silver atoms are in their zero oxidation state within the escape depth investigated. The presence of S2p at 164 eV is in agreement with the thiolate structure at the surface.[13a] No beam-induced damage[25] or oxidation of the clusters was seen in the time scale of the experiment. C1s appears at 285 eV, as in the case of 2D SAMs.[13a]

Infrared Spectroscopy. Fourier transform infrared spectra of the clusters are shown in Figure 5. The C−H stretching (A) and low frequency (B) regions are shown separately. The position of the methylene vibrations has been taken as a measure of the order (crystallinity) of the alkyl chains. In the case of crystalline polyethylene, the frequencies of the symmetric (d^+) and antisymmetric (d^-) CH_2 modes are at 2850 and 2920 cm^{-1}, respectively.[26] These values blueshift to 2856 and 2928 cm^{-1} in solution, respectively. This increase corresponds to greater number of gauche defects. For 2D SAMs, crystalline-like behavior is found for chain lengths above C6.[14] A similar behavior is seen in the case of 3D SAMs on Au.[7e] A systematic shift is seen in our 3D SAM spectra. In the case of Ag−BT, d^+ and d^- occur at 2856 and 2920 cm^{-1}, respectively. In Ag−PT, the values shift to 2848 and 2919 cm^{-1}, respectively. In Ag−OT and Ag−ODT, the values do not undergo any more drastic shift; they lie within 2 cm^{-1}. At the same time, the methyl vibrations do not undergo a systematic shift. The r^+ and r^- bands lie at almost similar values of 2868 and 2957 cm^{-1}, respectively, throughout. Thus, orientational freedom exists for the chain termini.

All of the other bands can be assigned on the basis of *n*-alkane vibrations.[26,7d] The intensity of the methylene scissoring band at 1463 cm^{-1} increases with chain length, and the 1423 cm^{-1} band that is assigned to the methylene scissoring adjacent to Ag−S bond[7d] decreases in intensity (relative to the band at 1463 cm^{-1}). The scissoring mode positions do not show any systematic changes with chain length. The number of methylene wagging and rocking bands appearing between 1400 and 1200 cm^{-1} also increase in intensity with chain length. All of these features show that the chemical integrity of the alkanethiol is maintained during the cluster formation. The increase in the progression bands in the range of 1180−1300 cm^{-1} with chain length is indicative of crystallinity;[26] it also indicates that the microenvironment of the monolayers is similar to that of 3D and 2D SAMs on Au. The band at 1340 cm^{-1} in Ag−OT is attributable to the end gauche conformation. The bands at 1118 and 1068 cm^{-1} are assigned as $(C-C)_T$ and $(C-C)_G$ stretching modes, respectively. The high intensity of $(C-C)_G$ in Ag−BT indicates either a near-surface defect or an internal kink defect.[23]

The 700−800 cm^{-1} region is composed of two sets of bands. The first is due to methylene rocking and the other is due to C−S stretching. These two bands have been discussed in the literature.[7d] In agreement with the studies of Hostetler et al.,[7d] we find that the shorter chains, C4 and C5, show two rocking modes corresponding to TT and GT conformers. The rocking mode due to the GT conformer occurring at 722 cm^{-1} is particularly evident in Ag−PT. The longer chains show only the TT conformer. The in-plane CH_3 rocking (β) is clearly observed in Ag−ODT and Ag−OT.

There are two C−S stretching modes, but $(C-S)_G$ shows up as a distinct band only in Ag−OT. $\nu(C-S)_T$ shows up as a well-defined band in Ag−ODT. In all of the other clusters, this band occurs along with the methylene rocking mode. The position of the bands is similar to that in the Au SAMs.[7d] We assign the band at 699 cm^{-1} of Ag−ODT as due to $\nu(C-S)_T$ because, as the defects in the alkyl chains are removed upon repeated heating/cooling cycles,[20] the methylene rocking mode at 719 cm^{-1} undergoes splitting, as seen in the

(25) Colvin, V. L.; Goldstein, A. N.; Alivisatos, A. P. *J. Am. Chem. Soc.* **1992**, *114*, 5221−5230.

(26) (a) Snyder, R. G.; Strauss, H. L.; Elliger, C. A. *J. Phys. Chem.* **1982**, *86*, 5145−5150. (b) Snyder, R. G.; Maroncelli, M.; Strauss, H. L.; Hallmark, V. M. *J. Phys. Chem.***1986**, *90*, 5623−5630.

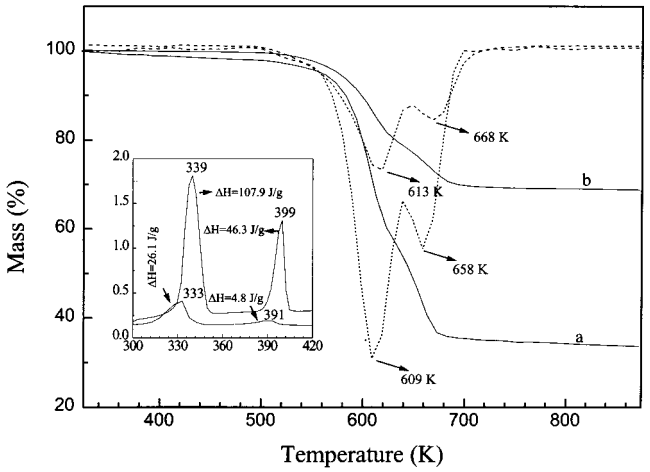

Figure 6. TG of (a) Ag−ODT and (b) Au−ODT. The first derivative of the weight loss is also plotted (dashed lines). The desorption temperatures are marked. Inset shows the DSC traces of (a) Au−ODT and (b) Ag−ODT (data upon warming). The transition temperatures and the enthalpies are marked.

case of hydrocarbon crystals,[27] showing that it has little contribution from ν(C−S).

Variable-Temperature Infrared Spectroscopy. At room temperature, the methylene (CH_2) symmetric (d^+) and antisymmetric (d^-) modes appear at 2847 and 2917 cm^{-1}, respectively, in Ag−OT, which is characteristic of crystalline alkanes.[26] These modes shift to 2855 and 2926 cm^{-1}, respectively, at 378 K (the values are those of liquid alkanes[26]). A drastic shift is observed corresponding to the melting of the alkyl chain. It is important to see that the phase-transition temperature (378 K) is higher than the value reported for Au clusters[10] and our own investigations of Au−OT. An increase in the alkyl chain melting temperature is suggested to be a signature of interdigitation.

Mass Spectrometry. Mass spectra of the clusters show peaks due to R^+, RS^+, $RSSH^+$ and $(RS)_2^+$, which are characteristic signatures of the thiol mass spectrum. In the absence of a disulfide band in the IR spectra, we attribute the $RSSH^+$ and $(RS)_2^+$ peaks to ion/molecule reactions upon desorption.Weak additional features are due to gas-phase association reactions. Desorption occurs around 553 K, similar to Au clusters[4] and comparable to TG data (see below). Only simple desorption is seen, and no degradation products are observed. Desorption leaves Ag at the end of the experiment.

Thermogravimetry. Thermogravimetric data of (a) Ag−ODT and (b) Au−ODT are shown in Figure 6. Desorption commences at around 540 K in both samples and is complete around 680 K. In the case of lower chain length thiols, desorption commences early and is complete at a lower temperature. No mass loss is seen beyond this temperature up to 900 K. In both Au−ODT and Ag−ODT, weight loss occurs through a two-step process, which we attribute to different adsorption sites at the surface for the thiolate due to the presence of different crystallographic planes. The two-step desorption pattern is different from those reported in the literature.[7a] In lower chain thiol-capped clusters, however, we see only one distinct weight loss. The weight loss is 46% for Ag−OT and 64% for Ag−ODT; both values are higher than those of the corresponding Au samples. Although there can be some contribution to this from the phase transfer reagent, there appears to be increased packing density in this material.

Differential Scanning Calorimetry. The phase transitions of the superlattice were investigated by DSC. The measurements were done in the temperature range of 123−473 K for all the samples, and the data for Au−ODT and Ag−ODT are shown in inset of Figure 6. There are no processes outside this temperature range. The data for the Au samples agree with the literature reports.[7a] The first peak corresponds to the melting of the alkane chains, and the second is due to that of the superlattice. Although the Au sample also shows a small peak corresponding to a superlattice melting, the energy values are higher for the Ag sample, corresponding to a greater fraction of superlattice in the sample. Both transitions occur at a higher temperature in Ag than in Au. It is seen that the superlattice melting enthalpy is comparable to that of the alkane melting, signifying large cohesive energies, as suggested by the molecular dynamics calculation.[28] A major contribution to the enthalpy of superlattice melting is associated with the interchain interactions and is not due to the intercluster core interactions.[28] The increased monolayer melting enthalpy in the silver cluster compared to that of the gold is in accordance with the increased organic fraction present in the material. However, the increase in energy is more than the increase in the fractional coverage. This is seen in both Ag−OT and Ag−ODT; we interpret it as being due to the superlattice, which makes an increased order within the monolayer bundles possible. Upon cooling (after being heated to 473 K), the superlattice melting peak completely disappears in Au and Ag. However, when the sample is heated only to 423 K and subsequently cooled, the superlattice melting is still observable in Ag−ODT, although the enthalpy reduces substantially.[20] This is in agreement with the in situ variable-temperature XRD investigations (vide supra).

Conductivity. Ohmic conductivity showed drastic dependence on the chain length. All conductivity measurements were taken on molten (at 398 K) and compacted disks. Although the room temperature conductivity of Ag−PT was on the order of $3 \times 10^6\ \Omega^{-1}\ cm^{-1}$, it was about $6 \times 10^6\ \Omega^{-1}\ cm^{-1}$ for Ag−OT. The value of Ag−ODT was above $10^7\ \Omega^{-1}\ cm^{-1}$. The variable-temperature conductivity data of Ag−PT and Ag−OT in the range of 298−398 K are shown in Figure 7. The conductivity showed significant variation upon repeated measurements on the same sample, and deviations between successive measurements were higher in the case of Ag−PT. The melting of the superlattice is quite evident in the conductivity data, the liquid phase shows a much larger temperature dependence. Upon fitting of the variation to a linear Arrhenius plot, activation energies of 46 and 306 kJ/mol were obtained for Ag−OT for the solid and liquid phases, respectively; the value for the solid phase is comparable to that of Au−OT.[7a] Almost negligible temperature dependence is

(27) Colthup, N. B.; Daly, L. H.; Wiberley, S. E. *Introduction to Infrared and Raman Spectroscopy*; Academic Press: New York, 1975; p 232.

(28) Luedtke, W. D.; Landman, U. *J. Phys. Chem.* **1996**, *100*, 13323−13329.

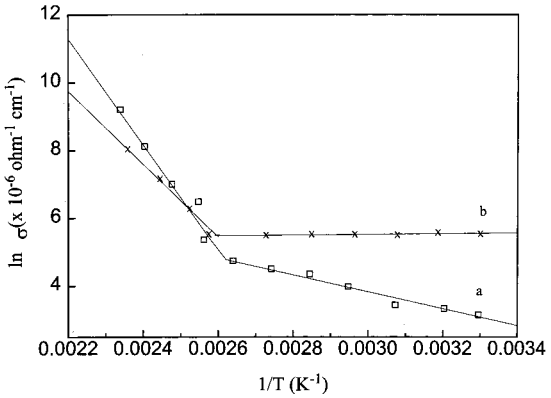

Figure 7. Variation of electrical conductivity with temperature of (a) Ag−OT and (b) Ag−PT. The transition corresponds to superlattice melting. The data have been subjected to a least-squares fit.

observed for Ag−PT up to melting, beyond which the conductivity increases significantly.

Investigations in the Solution Phase. *Optical Absorption Spectroscopy*. Optical absorption (extinction) spectra of octadecane-, octane- and pentanethiol-protected clusters are shown in Figure 8A. The solutions were prepared in $CHCl_3$. The peak maxima corresponding to the plasmon excitation[29] occurs around 424 nm in all of the clusters, indicating that the cluster sizes are similar. It is important to note that the width of the peak is slightly increasing with chain length. For comparison, the corresponding spectra of the solid films are also shown in the same figure (dotted lines). All of the spectra redshift and significantly broaden upon condensation. The extent of redshift is larger in Ag−PT and Ag−OT.

The redshift in the plasmon excitation frequency can be related to change in the dielectric constant of the medium surrounding the cluster. The classical plasma frequency is proportional to $(Ne^2/Km\epsilon_0)^{1/2}$, where N is the density of free electrons, e and m are the charge and mass of the electron, respectively, K is the dielectric constant, and ϵ_0 is the permittivity constant. In the clusters from C5 to C18, the core size of the clusters is about the same. It is likely that the adsorption-induced changes in the charge carriers will be the same in solution and in solid. Thus, upon condensation, the dielectric constant around the core increases and the peak redshifts. The change is not drastic in the case of Ag−ODT as the chain length is larger, and therefore, the change in the dielectric constant of the medium is not substantial. It appears that most of the chain length is solidlike in solution as well.

Another important aspect is the peak width. The peak width is related to the free electron collision time, and it is seen that, as the particle size decreases, the peak width increases corresponding to a decrease in the collision time corresponding to the confinement of electron motion within the cluster.[30] Upon condensation, line narrowing is expected due to increased electronic interaction between the clusters, but the observed behavior is the opposite. It is important to note that the increase in line width is larger for PT and OT but not for ODT. Clearly, there are additional factors affecting the excitation spectra.

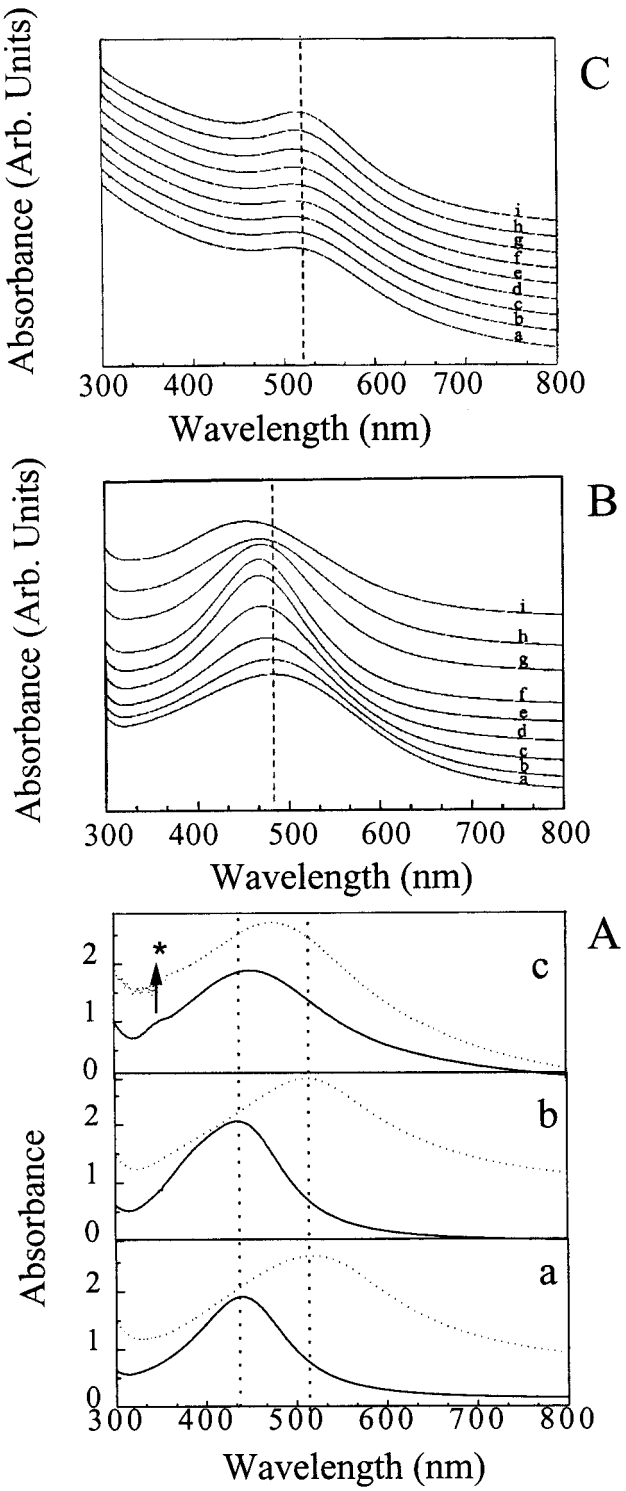

Figure 8. (A) UV/vis spectra of (a) Ag−PT, (b) Ag−OT, and (c) Ag−ODT. The solution (full line) and solid state (dashed line) data are compared. * Shows peak due to instrumental error. (B) and (C) show the temperature-dependent UV/vis of Ag−OT and Au−OT, respectively: (a) 283, (b) 293, (c) 303, (d) 313, (e) 323, (f) 333, (g) 343, (h) 353, and (i) 363 K.

Variable-Temperature UV/vis. In Figure 8B, the variable-temperature UV/vis absorption spectra of Ag−OT in the temperature range of 283−373 K are presented. The spectra were taken in toluene solutions, and the concentrations were well below the saturation

(29) Henglein, A. *J. Phys. Chem.***1993**, *97*, 5457−5471.
(30) (a) Kriebig, U.; Genzel, U. *Surf. Sci.* **1985**, *156*, 678. (b) Mulvaney, P. *Langmuir* **1996**, *12*, 788−800.

solubility of the clusters. No precipitation was observed during the experiment. The peak positions are slightly different from that in chloroform due to differences in the dielectric constant of the medium. In the temperature range of 283−323 K, the peak gradually narrows, and beyond this temperature, it broadens. Initially, there is also a blueshift of the peak maximum, and thereafter, it is almost constant.

Width of the peak is related to the collision time or the characteristic scattering of the oscillating charges as mentioned above. As the particle size decreases, the peak broadens. This is understandable because the charges are localized within the cluster. We interpret the data in the following fashion. At 323 K, the alkane chains have significant mobility and there is intercluster interaction, making the existence of aggregates of clusters possible in solution. This increases the scattering length, and the peak narrows. As the temperature is further increased, the intercluster interactions weaken, making the particles separate. The scattering length decreases, leading to an increase in the width. There can be a combination of effects affecting the bandwidth as well as position, leading to the reduction in intensity at lower temperatures. The intercluster interaction is influenced by the energetics of the interaction between alkyl chains of the adjacent clusters, thermal energy available, and the organization of the alkyl chains within the cluster. Upon cooling, the changes are not reversible. This suggests irreversible aggregation.

To see whether such an effect is seen in Au−OT, the UV/vis spectrum as a function of temperature was measured (Figure 8C). No significant change is seen in either intensity or position with temperature. We propose that this difference is due to the poor mobility of alkyl chains in Au−OT. The increased mobility of alkyl chains in Ag−OT makes interdigitation of the monolayers possible, explaining the changes in the variable-temperature UV/vis spectra. Ag−ODT and Au−ODT behave similarly.

Nuclear Magnetic Resonance Spectroscopy. We see that the ordering of the alkyl chains in the solid state is comparable to that of crystalline alkanes. In solution, however, the situation could be different. The formation of interdigitated superlattice solid implies that the alkyl chains could be interacting even in solution, as suggested by the UV/vis measurements. We thought that such a difference would be manifested in their diffusion coefficients. The methodology employed is discussed in the literature.[21] The values of diffusion coefficients obtained for Ag−OT and Ag−ODT are 1.0557 and 0.8637 ($\times 10^{-5}$) cm^2 s^{-1}, respectively. To make a comparison, the corresponding values of Au−OT and Au−ODT, prepared under identical conditions were measured, and the values obtained were 5.2782 and 1.1586 ($\times 10^{-5}$) cm^2 s^{-1}, respectively. An increase in the value of Au clusters is expected because the core dimension is smaller than that in Ag. However, there is another important aspect. Although there is a 4.58-fold reduction in the value of Au−ODT compared to that of Au−OT, the reduction is only 1.12 times in Ag. It has to be remembered that the core size of a given metal is approximately the same for OT- and ODT- capped clusters. This implies that the relative increase in total (core + ligand) cluster size in the two samples is lower for Ag than for Au. We attribute the difference to an increase in the effective cluster size due to the presence of intercluster interaction in Ag and the absence of it in Au. Because of the presence of such interactions, the relative increase in the effective size in Ag with increasing chain length is not as much as in Au. Note that the superlattice unit cell dimension increases only to a smaller extent (from 59.172 (Ag−OT) to 67.465 (Ag−ODT) Å) while the isolated cluster radius (core + ligand) increases from about 27 (Au−OT) to 42 (Au−ODT) Å. Thus, the relative increase in dimension is larger in the case of isolated clusters. Although this argument is rather crude, it seems to explain the experimental facts.

In proton NMR spectra, the peaks are downshifted upon adsorption. The spectra show two characteristic sets of peaks due to methyl and methylene protons. The methyl triplet appears at 0.84 ppm in the cluster (the lines are split due to the presence of two kinds of methyls, one involved in interaction and the other that is free), and the methylenes manifest as three peaks at 1.19, 1.23, and 1.31 ppm. The width of the peaks is related to the relaxation mechanisms and the type of binding sites at the surface.[4] The peaks broaden when the methylenes get closer to the cluster surface; as a result, α methylene is not observed as reported before.[4] As the chain length of the thiol decreases, the line width of these peaks increases; thus, the peaks are broader in OT than in ODT. Both Au and Ag clusters behave similarly in this regard. Increasing the temperature to 343 K does not change the spectrum drastically except for the methylene closest to the surface, which manifests increased broadening. The splitting of the methyl triplet is still observable in the spectrum, suggesting the existence of intercluster interaction, although there is a reduction in intensity. A general agreement between the UV/vis, NMR, and diffusion data seem to suggest that this interpretation is correct.

Summary and Conclusions

This study has shown that interdigitation of monolayers leads to the formation of superlattice solids. Interdigitation had been proposed earlier with 3D monolayers, but the formation of single-phase superlattices as bulk solids in a simple procedure is reported for the first time. Superlattices of monolayer-capped clusters have been observed in semiconductor nanocrystals,[31] thiol-capped metal clusters,[15,32] and Langmuir−Blodgett films of clusters.[3d] Analysis of the XRD pattern suggests that interpenetration of bundles of monolayers is the possible reason for the formation of such organic-assembled metal solids. Corroborative evidence is presented for the existence of interdigitation from variable-temperature FT-IR spectroscopy, optical absorption spectroscopy, and NMR. Measurements suggest that interactions between monolayers occur in solution as well.

The principal question is why such structures are formed with Ag but are not observed with Au. The

(31) Murray, C. B.; Kagan, C. R.; Bawendi, M. G. *Science* **1995**, *270*, 1335−1338.

(32) (a) Whetten, R. L.; Khoury, J. T.; Alvarez, M. M.; Murthy, S.; Vezmar, I.; Wang, Z. L.; Stephens, P. W.; Cleveland, C. L.; Luedtke, W. D.; Landman, U. *Adv. Mater.* **1996**, *8*, 428−433. (b) Wang, Z. L. *Adv. Mater.* **1998**, *10*, 13−30.

answer appears to be associated with the adsorbate structure of the thiolate group and the kind of crystal planes existing at the metal cluster surface. The angle of tilt for thiolates on Ag is smaller (∼0−17°) compared to that on Au (∼30°).[28,33] This smaller tilt makes interdigitation more probable in Ag, leading to extended superlattice structures. However, this adsorbate geometry corresponds to 2D SAMs, which cannot be directly adapted to the 3D SAMs. As revealed by MD simulations[28] on small clusters, the alkyl chains predominantly arrange to form bundles. It appears that these bundles are existing even in solutions of the clusters. The fact that even sudden precipitation of the clusters results in the formation of superlattices suggests that the kinetics of self-organization as in the case of 2D SAMs is not important here. It is clear from the infrared spectra that the alkyl chains are fully extended and assume an all-trans conformation. It is unlikely that such a conformation is achieved throughout the solid on a subsecond time scale given the fact that 2D self-assembly occurs on the time scale of hours.[24] Thus, it is likely that the alkyl chain order is not altered during the formation of the superlattice solid. This means that most of the cohesive energy of the superlattice solid arises from the interdigitation of bundles. Clearly, a cluster surface with more planar low-index faces will only promote bundle growth. More work is needed to understand the cluster surface morphology to answer this question.

Because such single-phase superlattices are possible under a variety of conditions and with a range of alkanethiol chain lengths, it should be possible to find cluster superlattice solids with other metal−adsorbate systems as well. Therefore, this class of materials should form a different set of "molecular solids". Under careful preparatory conditions, it might even be possible to make superlattice single crystals. Such solids will allow the investigation of a range of properties, and some of them may indeed be novel. These aspects are under investigation in other laboratories as well.[15,34]

Acknowledgment. T.P. thanks the Department of Science and Technology, Government of India, for supporting his research program on monolayers. N.S. and M.R.R thank the Council of Scientific and Industrial Research for Research Fellowships. Part of this research was done in Purdue University when T.P. was a Senior Fulbright Fellow in the laboratory of Prof. Graham Cooks. Technical help from Mr. M. S. Moni (NMR) and Dr. Said Mansour and Mrs. Kanjanamala (TEM) is acknowledged.

CM990429T

(33) Fenter, P.; Eberhardt, A.; Eisenberg, P. *Science* **1994**, *266*, 1216.

(34) Collier, C. P.; Vossmeyer, T.; Heath, J. R. *Annu. Rev. Phys. Chem*. **1998**, *49*, 371−404.